Electrochimica Acta 468 (2023) 143201

Contents lists available at ScienceDirect

Electrochimica Acta

journal homepage: www.journals.elsevier.com/electrochimica-acta

Design and analysis of a low-cost potentiostat for application with microbial electrochemical sensors

Andrew Hill [a,*], Stephan Tait [a], Peter Harris [a], Craig Baillie [a], Bernardino Virdis [b], Bernadette K. McCabe [a]

[a] Centre for Agricultural Engineering, University of Southern Queensland, West Street, Toowoomba, QLD 4350, Australia
[b] Australian Centre for Water and Environmental Biotechnology, The University of Queensland, St Lucia, Brisbane, QLD 4072, Australia

ARTICLE INFO

Keywords:
Electronic circuit
Sensing
Anaerobic digestion
Volatile fatty acids
Acetate

ABSTRACT

Potentiostats are often limited to relatively costly laboratory-based analysis, which limits their access and application by researchers and practitioners, including for mobile in-field systems. This paper presents an alternative low-cost potentiostat design, sufficiently accurate for application with a microbial electrochemical sensor. The design of the device is described, evaluated using simulation and applied to a microbial electrochemical sensor to measure acetate. Incorporated into the design are a micro-controller, local data storage, and a standard industrial communication protocol to provide flexibility and data management. The device was able to produce a potential at ±2.5 V relative to an Ag-AgCl reference electrode and to measure current at ±2 mA, which was comparable to the performance of laboratory potentiostats on the market. Simulation analysis using fundamental electronic principles, such as Ohm's Law, confirmed that operation of the system was valid and as expected. Further testing using a pseudo-cell showed the device was accurate across a relevant potential range. Results from the initial calibration of the device show less than 1.6 % standard error of the mean. The device was further applied to a microbial electrochemical cell to measure acetate, which confirmed the device was functional for this application and recorded values were consistent with expectations based on the relevant literature.

1. Introduction

Microbial electrochemical technologies (MET), use microorganisms to produce electrical energy from organic substrate [1], and can be relatively simple and affordable; however, the measurement device, a potentiostat, is often sophisticated (e.g., multichannel), tailored to highly controlled laboratory investigations, and relatively costly. Although smaller, single-channel potentiostats can be purchased, accessibility may still prove to be prohibitive, and may hinder research progress and industrial practice. In keeping with a simple and affordable MET approach, the supporting measurement device should also be economical and accurate. Several potentiostat circuits have been produced using a microcontroller (μC) and common electronic components which have demonstrated accurate analysis at a relatively affordable cost [2–5]. However, there is often a trade-off whereby cheaper potentiostats reduce functionality, resolution, and application.

In the context of microbial electrochemical sensors (MESe), which play a vital role in various research fields including biogas energy production via anaerobic digestion, the combination of an MESe with a potentiostat enables precise control of the cell potential and facilitates high-resolution current measurement [6–8]. This approach eliminates the limitations associated with external resistance methods and allows for more accurate analysis of volatile fatty acids (VFA), which serve as stability indicators in anaerobic digestion processes [6,9,10].

Microbial electrochemical measurement methods vary but can be typically separated into two groups; resistive [11,12]; and potentiostatic [7,8]. The resistive method involves a resistor(s) applied to the cell [13,14] and, similar to chronoamperometry, the current is determined by applying Ohm's Law. However, external resistance inherently increases cell resistance and thereby reduces cell performance [15], removes control of the electrochemical cell environment, and negatively affects microbial community growth [9,10].

To minimise the cell error due to electrolytic resistance and other parasitic characteristics, a potentiostat can be used in conjunction with a 3-electrode cell. The potentiostat regulates an electrolytic cell's potential relative to a reference electrode (RE), thereby reducing unwanted

* Corresponding author at: Centre for Agricultural Engineering, University of Southern Queensland, West Street, Toowoomba, QLD 4350, Australia.
E-mail address: Andrew.hill@usq.edu.au (A. Hill).

https://doi.org/10.1016/j.electacta.2023.143201
Received 6 April 2023; Received in revised form 22 July 2023; Accepted 13 September 2023
Available online 14 September 2023

effects (e.g., resistance) and achieve maximum efficiency [15]. The combination of a potentiostat and an MESe enables accurate control of the cell potential concomitantly allowing high-resolution measurement, and is often the primary method to obtain quantifiable data from an MESe [16,17].

Low-cost potentiostats can be built around a low-cost microcontroller, which allows for greater flexibility in experimental design. Microcontrollers can provide additional functionality by allowing parameters, such as electric potential range, voltage sweep rates, time-stamped values, and wireless networking to be modified/added as needed [5,18]. Arduino's integrated development environment compatible microcontrollers are commonly used, although direct use of onboard peripherals such as analog to digital converters can limit operating resolution and capabilities [5,19]. This highlights that an accurate and precise low-cost potentiostat will require a combination of low-cost microcontroller and low-cost supporting components.

Commonly found in the literature for low-cost potentiostats are studies aimed at low-cost (≈$50 USD) potentiostats for teaching [18, 19]. Potentiostats in a teaching context can be simple and low-cost but can be limited in resolution and accuracy, which may be tolerable in the teaching context. Teaching on potentiostats can provide valuable experience to students and demonstrates basic potentiostat operating principles and configuration. However, it is important to include potentiostat fundamental principles and relevant validation, which is often not reported [5,20]. It is possible for a potentiostat to be designed as low-cost and not sacrifice potentiostat resolution and accuracy.

This paper focuses on the design of an affordable yet accurate potentiostat for use in conjunction with an MESe (3-electrode cell), as this combination provides a controllable and efficient electrochemical cell environment. The design expands on previously identified circuits to provide a flexible, accurate, and low-cost potentiostat, that provides local and external (laptop) data storage. The potentiostat presented in this paper was designed to perform current vs. time measurements (chronoamperometry) and can be reprogrammed depending on application. This paper describes the design and analyses the performance of the potentiostat designed around the novel application of a cost-effective ultralow-noise instrumentation amplifier (in-amp). Simulation of the current measurement circuit utilising transimpedance amplification is provided along with measurements of current generated from acetate respiration in an MESe application. This demonstrates that a relatively affordable but versatile potentiostat can be designed that incorporates high accuracy and a simple design. This work aims to facilitate access to affordable and accurate potentiostats that support increasing research in MESe monitoring of AD systems, but also more broadly in the development of MET processes.

2. Materials and methods

All chemicals used were of an analytical reagent grade. Anaerobic digester sludge used for inoculation during testing of an MESe application was sourced from a domestic wastewater treatment plant previously described by Kazadi Mbamba, Flores-Alsina, John Batstone and Tait [21]. The inoculum was filtered prior to use with a 150 μm sieve to remove large organic and inorganic material. Media for testing was comprised of 50 mM phosphate buffer containing trace minerals and vitamins as described by Kim, Min and Logan [22].

2.1. Device

Input voltage noise and voltage noise density were selected as the primary selection criteria for the amplifiers used in the potentiostat design. These parameters were used to select components to limit noise in the potentiostat as potentiostats typically measure very small currents (i.e., 10^{-6} Amps) and are highly susceptible to interference. Other amplifier parameters that were considered before selection included input bias current, input offset voltage drift, and continuous output current. The selection criteria considered optimal values depending on the parameter, cost, and availability. A summary of these key characteristics for amplifiers is presented in Appendix A, Table A1.

The power requirement for each potentiostat was approximately 1 W, with the input voltage range being 5 – 24 V. Voltage supply to mounted components was via on-board regulators that produced ±5 V. The design of the potential range for the potentiostat was selected based on the anticipated experimental operating window and desired component parameters. The operating potential range was selected as ±2.5 V, and a maximum measurement current of ±2 mA was selected based on the trans-impedance amplifier (TIA) resistor (1000 Ω) and in-amp maximum output (35 mA). Although higher potentials and currents are possible, these values were also selected to limit noise and simultaneously maintain high resolution and simplicity.

To control the cell potential, the μC communicates a 16-Bit value to the digital-to-analog converter (DAC) via the I^2C communication bus. The DAC output signal is buffered and conditioned before reaching the counter electrode terminal (CE_t). The resulting current (to overcome cell resistance relative to the RE) is combined with reduction current to complete the biofilm oxidation reaction. From the working electrode terminal (WE_t), the current flow is measured by the TIA and conditioning circuit, while the biofilm oxidation current is fed back through the potentiostat to the CE_t circuit. An analogue-to-digital converter (ADC) after the TIA circuit converts the signal to an integer value which is communicated back via the I^2C bus to the μC for processing. The RE connects to the reference electrode terminal (RE_t) of the feedback circuit and can either be shorted to potentiostat common ground or combined with the differential input to the CE_t in-amp. Values are stored on an SD card by the μC for later retrieval. The design also incorporates a common data bus running RS485 (Modbus) and a parallel power bus enabling multiple potentiostats to be daisy-chained. Data is transferred from the Modbus master to a computer via Serial-USB.

An ATMEL328P – Arduino Pro-Mini was selected as the μC for simplicity, cost, and availability. Programming of the μC was performed using the Arduino integrated development environment (IDE) using C/C++ coding language. For simplicity, the Arduino IDE consists of a large open-source library for connection to peripheral devices and communication protocols. By utilising the Arduino IDE, the μC program can easily be modified depending on requirements and data storage. The μC can be purchased for around 10 USD and is supplied through most electronic and online stores, making the μC cost-effective and available to everyone. Incorporated into the design is the AD8429 in-amp for current sensing in a TIA configuration. To control the CE_t positive and negative voltages, the MAX5541 DAC is used. Both the ADC and the DAC are 16-Bit precision. All buffering operational amplifiers (op-amps) are of type MC33178.

2.2. Device simulation

Before assembly of the circuit, the design of the potentiostat was first simulated in LTspice XVII to determine circuit response and evaluate component values (Fig. 1). The circuit analysis was simulated on an ideal cell (Fig. 1, R1), the DAC was substituted with an ideal voltage source (variable DC supply), and all other components set as designed. Output of the simulation designated "ADC" connected to the input of the ADC circuit. A voltage sweep of ±2.5 V (10 mV steps) was performed across resistor R1 (Fig. 1) and the response values were recorded. This simulated circuit was evaluated to ensure the potentiostats fundamental operation was as expected and correct before the addition of other components, such as an ADC and power regulators.

The simulated circuit (Fig. 1) has the electrolytic cell (as in an MESe application) represented by a fixed resistor (R1), noting that a real electrochemical cell would have additional complex resistance and capacitance [23,24]. Simulating the two-electrode circuit initially provided a simplified framework for analysis, verification, and optimisation of the potentiostat design. It helped ensure that the fundamental

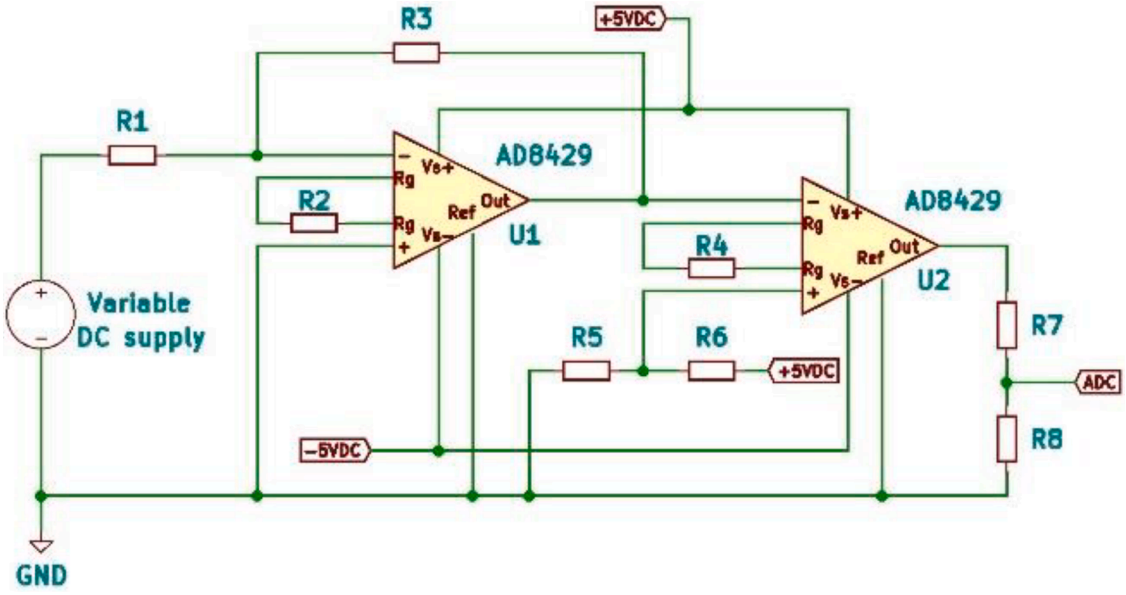

Fig. 1. Simplified circuit for simulation showing incorporated TIA current sensing, where: U1 & U2 are in-amps; R1 – R8 are resistors; U1 & R3 form the TIA circuit; R2 & R4 are gain selecting resistors; U2 and supporting connections are used for conditioning the electrical signals.

principles and performance of the circuit were understood and met the desired criteria before proceeding to the more complex three-electrode configuration.

2.3. Device evaluation

To evaluate the potentiostat design, the complete circuit was produced (Appendix A, Figure A1) on a printed circuit board and populated with components. In total, six potentiostats were assembled, and each test performed in triplicate. A 100 ± 1% Ω, 0.25 W resistor was placed across the CE_t and WE_t (RE_t shorted to circuit ground). Firmware was written in C++ (using the Arduino IDE) and uploaded to the μC to control the DAC output, the main loop function is presented below,

```
void loop() {
if (DACvalue >= 63,000) {
change = 0;
} else if (DACvalue <= 1000) {
change = 1;
} if (millis() - prevTime > sampleRate) {
prevTime = millis();
if (change) {
DACvalue += 1000;
} else if (!change) {
DACvalue -= 1000;
} writeDAC_SPI(DACvalue, DAC_CS_Pin);
}
}
```

The DAC in conjunction with an onboard reference voltage (2.5 V) was used to control the CE_t voltage. For this, the output values of the DAC were swept from 0 to 65,535 (2^{16}) in increments of 1000. An op-amp on the output of the DAC was used to amplify the signal by a factor two and introduced a DC shift, this enabled the input signal to the CE in-amp non-inverting input to swing between −2.5 and 2.5 V, with unity gain of the CE in-amp this produced between −2.5 and 2.5 V on the CE_t. Values from 0–32,767 represent the negative output voltage, and 32,768–65,535 represent the positive output voltage. Where each step represents a voltage (V) change and is expressed by Eq. (1), with 1000 steps approximately equal to 0.0763 V. The respective CE_t, WE_t, and TIA output values were recorded with a multimeter (Digitech QM1549), the recorded voltages were compared with the corresponding DAC value, and with the ADC value (ADC_v) recorded on the SD card.

$$DAC_{step} = V_{ref} / DAC_{res} \quad (1)$$

Where; DAC_{step} is the voltage change corresponding to one integer value change, V_{ref} is the circuit reference voltage (i.e., 2.5 V), and $DAC_{res}$is the resolution of the DAC (i.e., 2^{16} for 16-Bit).

2.4. MESe verification

To further evaluate the response of the potentiostat in an application, it was connected to an MESe. Sodium acetate (NaAc; 20 mM) was added and used as the sole carbon source in the tests. Initially, the cells were dosed with 10 mM NaAc but unfortunately, no measurable response was observed from the sensor (discussed further in Section 4.3). The NaAc concentration was increased to 20 mM (approximately 1,640 mg L^{-1}) and the cells were cleaned, fresh inoculum and media added, and the measurement restarted. Biofilms can tolerate high acetate concentrations [11], so the concentration of 20 mM was selected, and this produced a biofilm and a current signal. The cell was comprised of a 100 mL Schott bottle filled with 90 ml of electrolyte.

A custom 3D-printed cap of acrylonitrile-butadiene-styrene (ABS) to provide a gas-tight seal, thereby maintaining anaerobic conditions. The cap design incorporated rubber o-rings to seal the cap on the bottle and around the electrodes protruding through the cap. The distance between the electrode holes (WE and CE) was 20 mm (centre to centre). The RE location was offset from the CE by 15 mm, and the WE by 11 mm (Appendix A, Figure A2). A small safety vent (2 mm diameter) was also placed in the cap as a safety measure for any gas overpressure and sealed with silicone grease. Once assembled the cell was checked for water tightness by inserting all electrodes and seals, filling the bottle with water, and securing the cap. For this, the assembled cell setup was inverted and placed in a glass beaker and routinely checked for any droplets forming over 24 h.

The RE consisted of a silver/silver chloride (Ag/AgCl) wire immersed in Potassium Chloride (3 M KCl) saturated with AgCl (Sigma-Aldrich 60,137) and was housed in a glass tube with a CoralPor membrane (BASi MF-2042, USA). The constructed RE was calibrated against a standard Ag/AgCl electrode (BASi MF-2056, USA) to within ±10 mV.

The CE and the WE were both made from graphite rods (Morgan Advanced Materials), each with a diameter of 6.35 mm (1/4″) and were

cut to 120 mm in length. The WE and CE had an exposed surface area of 3.76 cm^2 and 19.71 cm^2 respectively. Graphite electrodes were prepared by firstly rinsing with acetone and subsequently sanding with 1200 grit sandpaper to produce a smooth uniform surface. The electrodes were then rinsed with deionised water (MilliQ), then acetone, and then dried with lint-free wipes to remove any loose debris from the electrode surface.

Three cells were constructed as above and were inoculated with anaerobic digester sludge sourced from a domestic wastewater treatment plant previously described by Kazadi Mbamba, Flores-Alsina, John Batstone and Tait [21]. The inoculum to media ratio and chronoamperometric settings are as previously described by Gimkiewicz and Harnisch [25]. Current measurements were recorded at 10-minute intervals and averaged across the 3 cells. After the initial inoculation period of 8 days, the buffer and NaAc mixture was exchanged every 4 days. After establishing sufficient current flow, the current values were measured for each feeding cycle (4 cycles). Testing was performed in an environmental chamber (CM Envirosystems, PAC-120-AH) maintained at 37 ± 0.5 °C.

2.5. Data analysis and statistical methods

Descriptive statistics were calculated using Microsoft Excel 365 (2021) Add-in Analysis ToolPak to determine the sample mean, standard deviation, and standard error of the mean (SEM). Linear regression analysis of each potentiostat's ADC_v against TIA voltage, and CE_t voltage against DAC value were also performed in Microsoft Excel.

3. Theory

Microbial respiration is used by MESe to liberate electrons in an electrocatalytic oxidative process that produces electrons which are measured in the form of current or voltage [26]. The current generated represents the oxidation of the electron donor (here being acetate) due to biofilm respiration. In the case of acetate respiration, eight electrons are liberated per molecule of acetate oxidised (Eq. (2)). According to Korth and Harnisch [15], an acetate-derived electroactive biofilm used in an MESe is most thermodynamically efficient at 0.2 V. This will impact the desired design range of a potentiostat and can influence the type of RE to be used.

$$CH_3COO^- + 4H_2O \rightarrow 2HCO_3^- + 9H^+ + 8e^- \quad (2)$$

3.1. Device circuit topology

The potentiostat is an electrochemical instrument that maintains a constant potential (voltage) between the working electrode (WE) and the reference electrode (RE) in an electrochemical cell, while measuring the resulting current. This is achieved through a feedback mechanism that continuously compares the measured voltage to a desired setpoint and adjusts the counter electrode (CE) current to maintain the desired potential at the WE [27,28].

A potentiostat's principle of operation involves an operational amplifier in a feedback loop configuration. The operational amplifier compares the measured voltage difference between the WE and the RE to the setpoint value and generates an output signal that controls the CE current. By adjusting the CE current, the potentiostat counteracts any deviation from the desired potential, thereby maintaining a constant potential at the WE [27,29].

In this study the specific design topology (Fig. 2) incorporates a TIA for current measurement, and a μC to allow for custom programming. Supporting components would also include operational amplifiers, an analog-to-digital converter, a digital-to-analog converter, data storage, and a communication network.

3.2. Component selection

Components were chosen to ensure robust operation in harsh environments and compatibility with existing wastewater management infrastructure for field deployment of the MESe. Component selection took into consideration factors such as temperature tolerance, noise immunity, resolution, and potential range. The trade-off between cost and performance was also considered during component selection. For example, one of the reasons the AD8429 was selected was the temperature range of −10 to 125 °C, which would give a high degree of confidence in measurements when exposed to fluctuating temperatures. Additionally, there were similar tradeoffs between input bias current and voltage noise density, for example, 150,000 pA and 1 nV/$\sqrt{Hz}$, respectively, for the AD8429 (this study), compared to other devices such as the AD8221 with 400 pA and 8 nV/$\sqrt{Hz}$. By selecting higher power consumption, a lower noise density was achieved. This choice

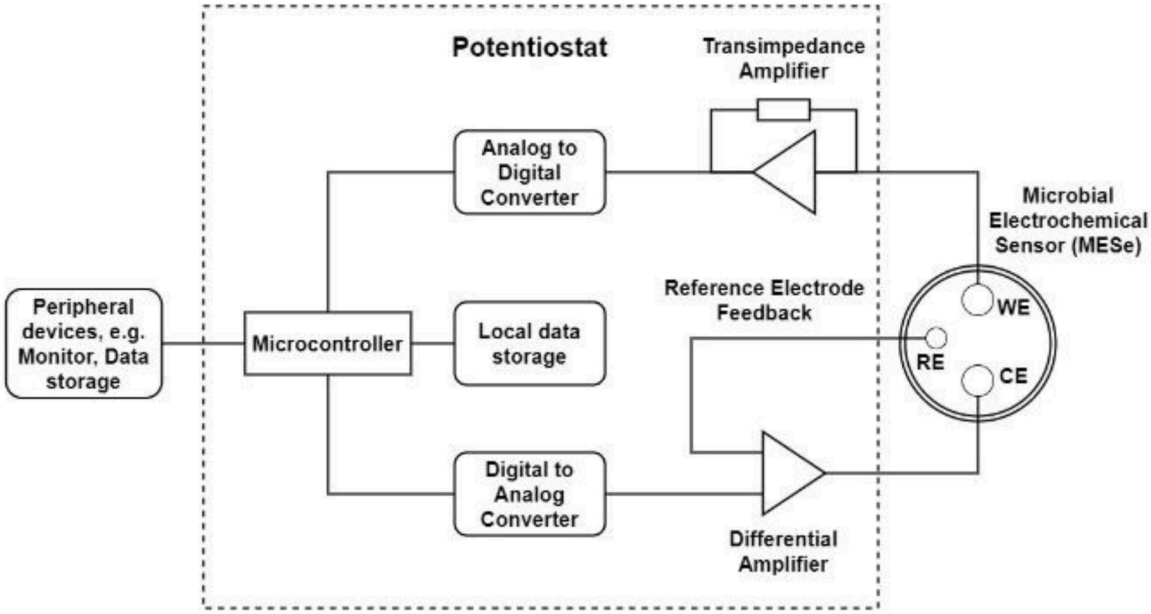

Fig. 2. Potentiostat operational flow with lumped elements.

came at a cost (literally), with the AD8429 costing approximately three times more than the AD8221.

3.3. Device operation

The potentiostat should be capable of meeting and/or exceeding the operational electrochemical potential to compensate for experimental conditions, such as cell geometry, electrode material, media conductivity, double-layer capacitance, and membrane diffusion resistance. To operate an MESe at the most thermodynamically efficient potential for VFA respiration/measurement, a minimum of ±0.2 V at the biofilm surface has been recommended [15], although additional range will be required to overcome cell resistance and capacitance. For example, a DAC (used to control the output potential) can require a reference voltage to function (in this case $V_{ref} = 2.5$ V), which limits the output range. The output from the DAC can be amplified to higher voltages but this will introduce additional unwanted noise and capacitance for each extra stage of the circuit, therefore it is best practice to use as little amplification as possible for the application. Consequently, for a common 5 V circuit and for one stage of amplification the output potential

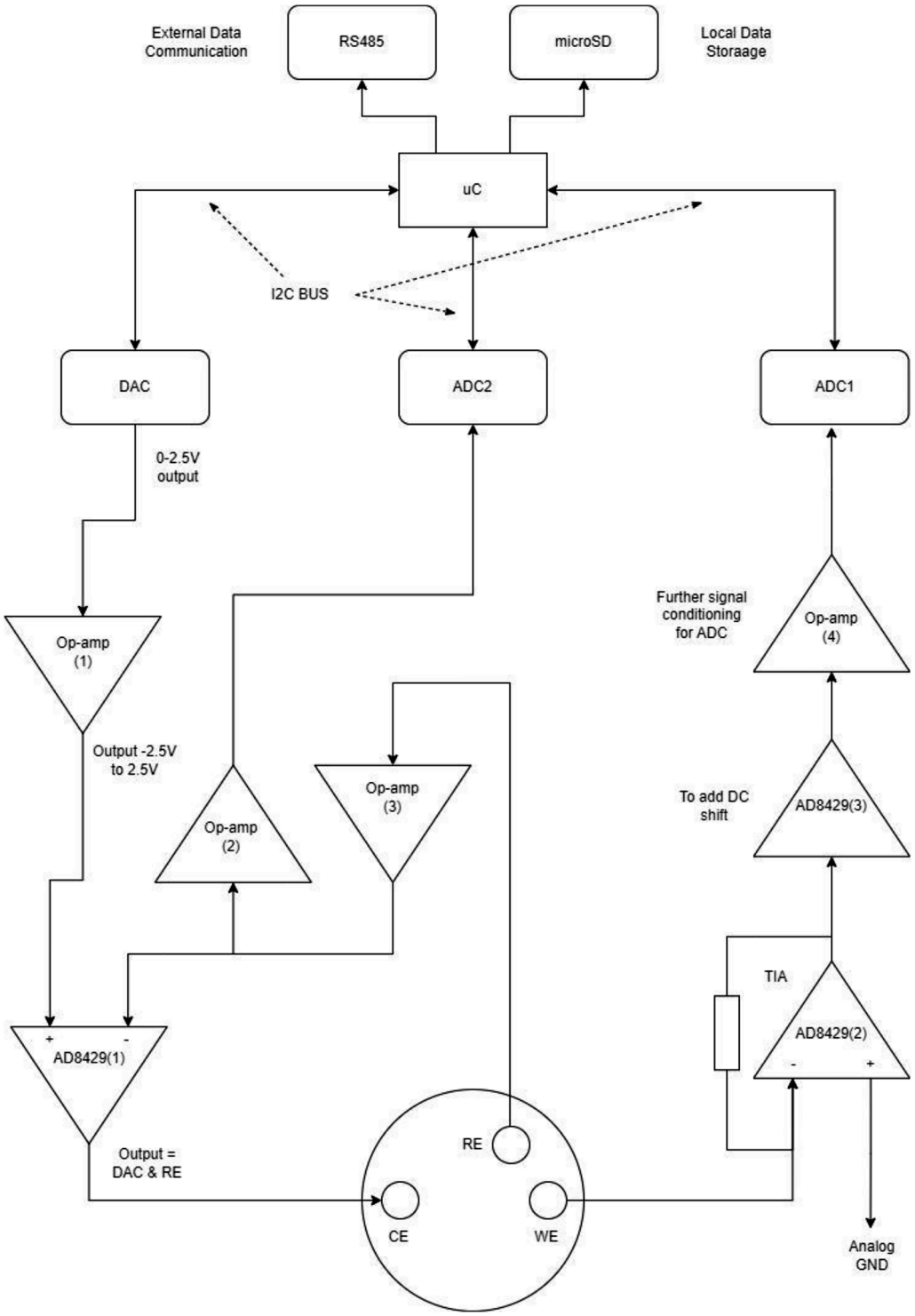

Fig. 3. Potentiostat design excluding supporting components such as voltage regulators and resistors.

would be ±2.5 V giving a differential range of 5 V. This would exceed the MESe recommended potential by more than 10 times, while enabling a broad range of applications.

Additionally, the current through an electrolytic cell and potentiostat needs to be sufficient to drive the reaction in Eq. (1), which is limited by the in-amps output and the TIA resistor selection. Current flow through the TIA resistor (Fig. 1) is used to determine the relationship between the input potential, electrochemical cell resistance, and biofilm current, while the in-amp sets the maximum current. The output measured at the point designated "ADC" in Fig. 1, represents the signal into the ADC circuit. The ADC converts the signal to an integer that represents the current flow through the cell. Current through a resistor representing the electrochemical cell (I_{cell}) can be represented using the output signal of the TIA in-amp and the virtual ground of the TIA circuit as follows (Eq. (3)):

$$I_{cell} = -\left(2V_{out} - V_{off}\right)/R_{TIA} \quad (3)$$

where V_{off} is the voltage generated from the voltage divider resistors R5 & R6 (Fig. 1), V_{out} is the voltage to the ADC after the voltage divider R7 & R8 (Fig. 1), and R_{TIA} is R3 (Fig. 1).

The potential from the half-cell of the RE (Fig. 3) is passed through the non-inverting input of an op-amp in voltage follower configuration. The op-amp input presents a high impedance, which minimises current flow through the reference electrode (a desirable effect). The output of the reference electrode op-amp is connected to the inverting input of the counter electrode in-amp. The RE voltage passes through to the non-inverting input of the CE in-amp and combined with the user's desired working potential set by the DAC via the firmware (in this case 200 mV), thus allowing automatic cell potential control via feedback from the RE. Additionally, the RE op-amp signal is connected via an additional op-amp and 16-Bit ADC (Fig. 3) for recording by the μC.

4. Results and discussion

Affordability is a key consideration in the design of a proposed potentiostat for future MESe applications, including monitoring VFA in anaerobic digesters. The potentiostat reported in this work had a minimal component cost of approximately 75 USD (Appendix A, Table A2), which included peripherals added to facilitate data collection (Fig. 3). Local data storage in the form of a microSD card and reader was added, as well as RS485 communication for external data storage. Power supply was not included in the potentiostat cost, the aim being to provide installation flexibility by allowing power to be provided from any low-noise low voltage source (e.g., battery, USB, solar, etc.). The cost of the unit compares well with other low-cost units [2,30,31], but cost is highly dependent on potentiostat parameters such as range, resolution, or functionality. The potentiostat design uses 16-Bit ADC in conjunction with low noise amplifiers (AD8429) to measure current accurately. The potentiostat uses industrial communication standards (MODBUS RS485), data storage redundancy, and narrowed potentiostat parameters to be more application-specific and aimed to facilitate the use of MESe in monitoring of anaerobic digesters for biogas energy production.

4.1. Circuit simulation

As expected, the voltage sweep produced a near-perfect linear response ($R^2 \approx 1.00$) (Appendix A, Figure A3). Over the applied voltage range, the simulated circuit voltages were within the design specifications. However, the simulation showed the output to the ADC tended to deviate from the linear relationship at 2.25 V and at -2.25 V. These deviations indicated a possible limit of operation for the proposed design, which was then explored during testing on the fully assembled potentiostat. Simulation confirmed the circuit functionality and that the voltage output from the TIA op-amp behaved as predicted when the voltage applied remained between ±2.25 V. Commercially available potentiostats may substantially exceed this operational range, which can provide additional development scope. Although, MESe applications will often only require a potential of several hundred millivolts and are quite often operated between ±1 V [16,17,32], and higher voltages (e.g., ±10 V) may not necessarily be required for MESe. Overall, the simulation suggested predictable and sufficiently accurate behaviour for the potentiostat design.

4.2. Pseudo-cell testing

To determine the accuracy and linearity of the potentiostat, a voltage sweep across the resistor between CE_t and WE_t was performed (Fig. 4). As expected, the recorded CE_t voltages showed a near-exact linear relationship against the DAC input value ($R^2 \approx 1.00$). The output from the DAC was predictable and accurate across all six replicate potentiostats.

The standard error of the mean (SEM) analysis showed that the variation ranged between 0.05% and 0.69%. The SEM increased somewhat asymptotically towards a CE_t of zero volts, which corresponded to a DAC value of 32,767. The SEM reached a maximum of 0.69% at 17.5 mV, resulting in an absolute error of only 0.12 mV. Despite the possibility of the error growing as the CE_t voltage approached zero, the accuracy of the potentiostat was deemed to be sufficient for the intended MESe application (e.g., AD monitoring).

The analysis of the WE_t voltage and ADC_v recorded by the μC during the voltage sweep revealed a discontinuous line (Fig. 5) in the raw ADC_v data due to the electronic shaping (Appendix A, Figure A4). To address this, the ADC_v was modified (ADC_m) by subtracting 65,535 from values over 32,767, allowing regression analysis and curve plotting.

A linear regression fit to the mean ADC_m values (Fig. 5) showed a statistically good fit ($R^2 \approx 1.00$). The SEM for ADC_m measurements ranged between 0.00% and 1.58%. The maximum SEM of 1.58% occurred at a WE_t voltage of 48 mV, approaching zero SEM as the voltage neared +2.1 V and -2.1 V. The SEM values exhibited asymptotic tendencies towards zero applied voltage, similar to the CE_t data.

The standard deviation (std. dev.) analysis of the ADC was graphed in Fig. 5, although, the values were visually indistinguishable from the data points. The relative std. dev. values ranged from 34.7 to 84.9 at an ADC_m of 22,037 and -31,810 respectively. The highest std. dev. occurred close to the maximum WE_t voltage, while the highest relative std. dev. corresponded to values approaching the zero applied voltage, with std. dev. of 6.7% at an ADC_m of 698.

The potentiostat was unable to produce WE_t voltages above 2.1 V or below -2.1 V, despite supply of ±5 V. However, the recorded values enabled the potentiostat to measure a range of ±2.0 mA which was within the design specifications for an MESe application.

The designed current resolution was calculated based on the range of the 16-Bit ADC and voltage range (5 V), resulting in a resolution of 76 nA. By using Ohm's law in combination with the linear regression fit of the data in Fig. 5, a relationship with the resistor current was formulated. Potentiostat resolution was better than expected, with an accuracy of 63 nA, corresponding to the maximum range produced from the assembled potentiostat (4.2 V).

The accuracy of 63 nA for the potentiostat refers to its ability to measure current with precision. It means that the potentiostat can detect and resolve current changes as small as 63 nA. This level of resolution is significant for applications that require the measurement of small current variations.

When comparing this resolution with commercially available instruments, it is essential to consider the specific requirements of the application. High-end potentiostats used in research laboratories can offer even higher resolutions, typically in the sub-nanoampere range. These instruments are designed for precise and sensitive electrochemical measurements, but they are often expensive and may not be suitable for all applications.

On the other hand, lower cost potentiostats or handheld devices

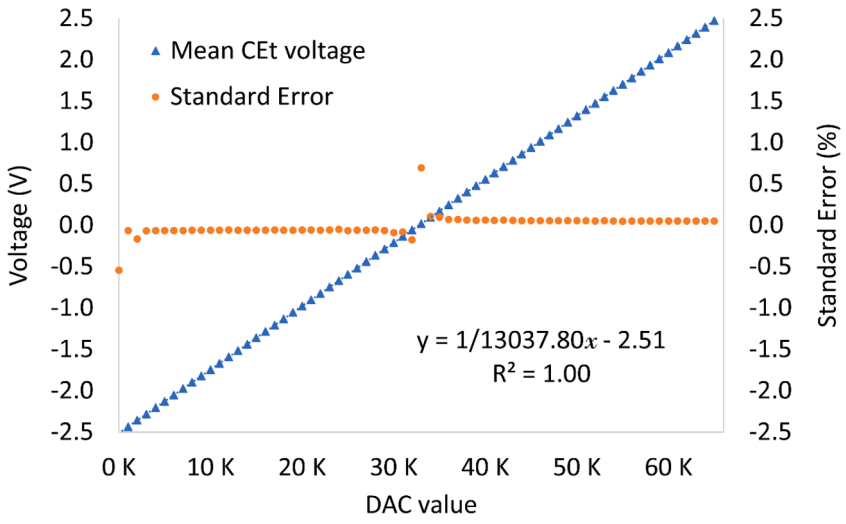

Fig. 4. Defined 16-Bit DAC value with measured response CE_t voltage (▲) across all 6 potentiostats. Standard error of the mean (●) shows change around 16-Bit DAC zero point (32,767).

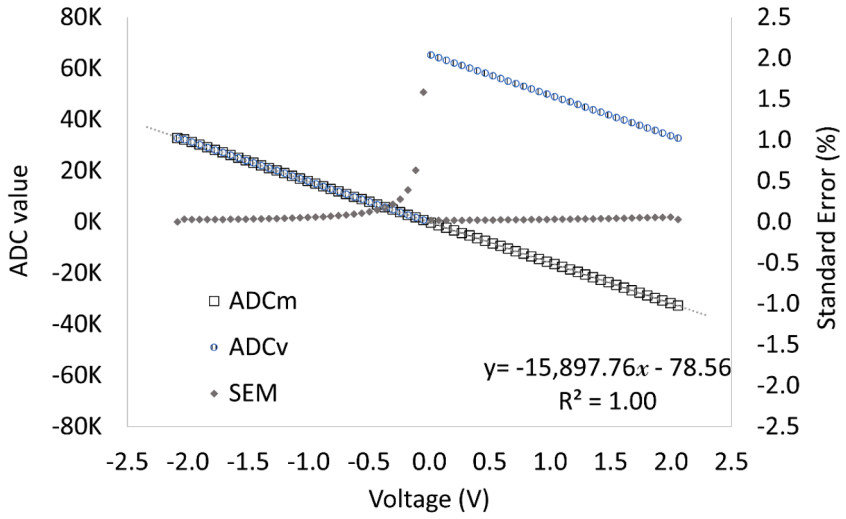

Fig. 5. ADC_v in response to WE_t voltage measured across 6 replicate potentiostats. The mean value is presented for both the raw ADC_v (○) and the ADC_m (□), together with standard error of the mean (◆).

intended for field use may have lower resolutions, typically ranging from microamperes to milliamperes. These instruments are more suitable for general monitoring purposes or applications where higher precision is not critical.

While the pseudo-cell test provided valuable insights into the potentiostat's performance, it is important to further evaluate the device using a real electrochemical cell. Testing the potentiostat with a well-known reaction, such as the ferri-ferro cyanide system, would provide a more comprehensive demonstration of its capabilities and further validate its performance.

The potentiostat demonstrated appropriate accurate measurements and linearity across a range of tested voltages, with SEM and std. dev. Values falling within acceptable limits. The potentiostat design was deemed appropriate for providing control of the cell potential and accurate current measurements in an MESe application.

4.3. Laboratory test with a microbial electrochemical sensor (MESe)

In this study, it was mentioned that initially, the cells were dosed with 10 mM sodium acetate (NaAc), but no measurable response was observed from the sensor. This could be due to the concentration of acetate being below the detection limit of the potentiostat/sensor system.

A higher resolution potentiostat system would have a lower limit of detection, meaning it can detect lower concentrations of analytes with a measurable signal. In the case of the study, increasing the NaAc to 20 mM resulted in a measurable response from the sensor. This suggests that the potentiostat/sensor system was more sensitive to the higher concentration of NaAc and was able to detect and measure the associated electrochemical activity.

However, the potentiostat does not directly measure the NaAc, but rather the electrons produced from the electro-respiring biofilm. The lack of a measurable signal at 10 mM sodium acetate (NaAc) could also be attributed to the absence or competition from non-electro-respiring bacteria in the system. In a mixed microbial community, other non-electro-respiring bacteria may be present and could outcompete the electro-respiring bacteria for the available acetate. Increasing the NaAc concentration to 20 mM likely provided a surplus of acetate that favored the electro-respiring bacteria, allowing them to outcompete the non-electro-respiring bacteria and establish a biofilm capable of generating a measurable current.

By monitoring the current output from the MESe, the oxidation of

NaAc and the activity of the biofilm can be quantitatively assessed. The electrochemical reaction occurring in the MESe is the oxidation of sodium acetate (NaAc) by the biofilm on the anode.

Sodium acetate, as a soluble organic compound, diffuses from the surrounding electrolyte into the biofilm on the anode surface. Within the biofilm, electroactive microorganisms, such as *Geobacter spp*., utilize NaAc as an electron donor. The biofilm contains specialized bacteria capable of transferring electrons from the oxidation of NaAc to the electrode surface [32–34].

At the electrode surface, the electroactive microorganisms oxidize NaAc, releasing electrons and protons. The acetate ion (CH_3COO^-) is converted to carbon dioxide (CO_2) and water (H_2O) during this oxidation process [33,35]. The released electrons from the oxidation reaction travel through the conductive biofilm and reach the anode, where they are collected. The magnitude of the current is proportional to the rate of NaAc oxidation by the biofilm [35]. The flow of electrons from the biofilm to the anode leads to the generation of an electric current, which is measured by the potentiostat (Fig. 6).

An MESe was assembled as described in Section 2.1. The output from the potentiostat (Fig. 6) showed typical biofilm growth behaviour, with an initial lag phase with near-zero current generation typical of biofilm establishment, followed by an exponential increase in the current flow at approximately 220 h, and later, a stationary phase. The stable current output reflects a steady-state condition where the rate of NaAc oxidation is balanced by the supply of NaAc and the metabolic activity of the biofilm [36].

In this study, the authors suggest the presence of *Geobacter spp*. based on the reddish-brown tint observed on the anode (Fig. 7), which is commonly associated with Geobacter biofilms [33,34]. However, further analysis would be needed to confirm the exact electrochemical reactions and microbial species involved in the MESe system.

Subsequent cycles of NaAc addition, the cell demonstrated a typical current curve with the initial peak in current (due to addition of NaAc) was followed by a stable current output, and finally, substrate-limited decline in current generation (Fig. 6). Between days 10 and day 25, peak values were recorded between 0.080 - 0.093 mA cm^{-2} and the mean current output was 0.068 mA cm^{-2}. Although, these values are somewhat lower than other values reported in the literature [16]; this could have been due to non-sterile conditions, which possibly promoting bacterial growth in the electrolyte consuming NaAc in the bulk liquid phase rather than by biofilm at the electrode (Fig. 7). This highlights the need for a high resolution and accurate potentiostat under such conditions, as measured currents may be relatively small. The potentiostat provided a high-resolution measurement of current fluctuations that were produced from the MESe biofilm with reproducible peaks in current being measured. Furthermore, the measured values were comparable with what is observed with other potentiostats measuring NaAc respiration at a fixed applied potential [35].

The current measurement of this potentiostat was lower than single chambered cells reported in the literature. For example, Kretzschmar, Koch, Liebetrau, Mertig and Harnisch [36] investigated MESe for sodium acetate measurement, and their sensor produced 0.569 ± 0.013 mA cm^{-2} which is much higher in the current study; although, the authors do identify the sensor response being highly dependent on prior acetate exposure [36].

Moreover, the current study investigated a primary biofilm, which is known to produce lower current densities than secondary biofilms [37, 38]. The cell output in the current study was comparable to what has been observed in microbial electrochemical cells with a membrane [39, 40]. A novel submersible sensor reportedly measured approximately 0.025 to 0.075 mA [39]. While Sun, Zhang, Wu, Dong and Angelidaki [41] reported a microbial cell producing a maximum of 0.1 mA cm^{-2} and a similar current response to NaAc as observed in the current work. A comparable response was also reported from a microbial electrochemical cell using a fixed applied voltage, which reached between 0.1 – 0.15 mA cm^{-2} for a comparable NaAc concentration [35].

Overall, the potentiostat described here was able to measure the biofilm response due to NaAc addition, and although lower current densities were observed than previously reported, the potentiostat was functional, including for an MESe application. Further studies using this potentiostat design and other NaAc concentrations, could provide additional data for comparison with the available literature.

5. Conclusion

Volatile fatty acids are a known indicator of AD stability. Previous MESe output signals demonstrated a correlation with VFA concentration and thus potential to be used applied to monitor AD. However, simple surrogate methods to a potentiostat, such as an external resistor to measure the current from an MESe was considered inadequate because of expected impacts on microbial communities and behaviour. Accordingly, a potentiostat is likely required to control the cell potential for electrochemical applications in general, and for stable cell environment and biofilm growth in MESe applications. Currently, a relatively low-cost and accurate potentiostat is lacking and this was a key need to enable MESe applications for more timely measurement of VFA in AD.

A potentiostat design was presented and evaluated for use in electrochemical analysis, developed based on the key considerations of affordability, simplicity, and robust measurements. A simulated circuit evaluation confirmed that the initial circuit design behaved as expected. Once assembled, the potentiostat showed good linearity when using a pseudo-cell (resistor), and the observed operation was within the desired

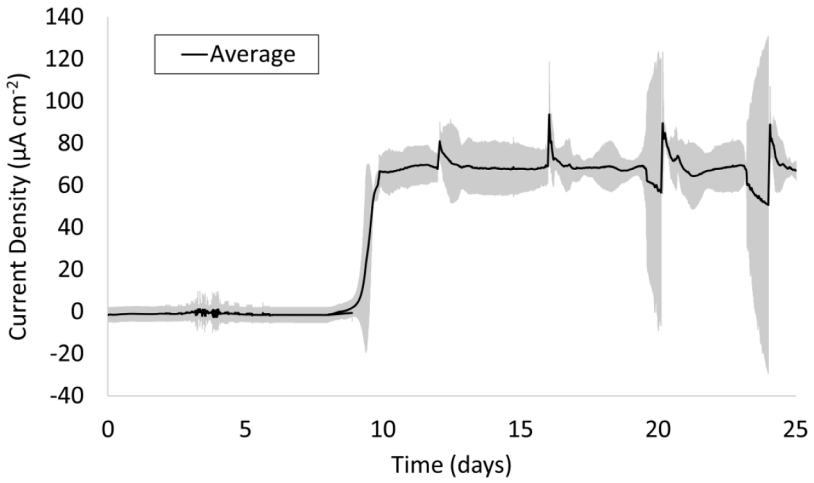

Fig. 6. Average signal output from biofilms (n = 3) over 25 days (600 h). Grey shaded area represents the standard deviation in replicate measurements.

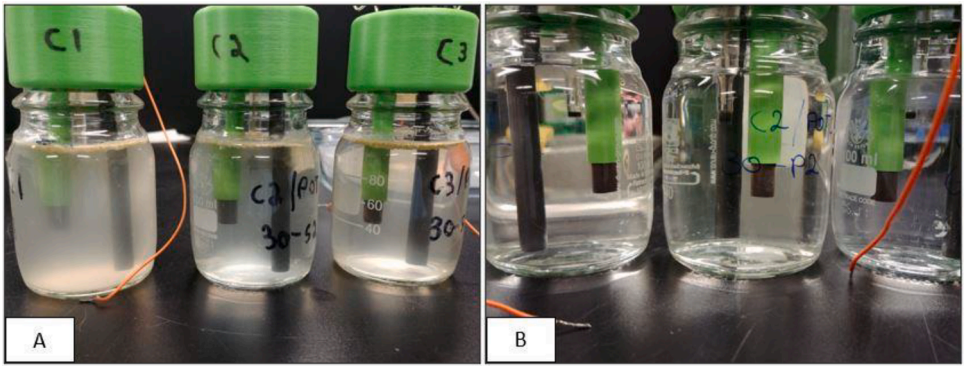

Fig. 7. Electrolytic Cells; (A) before and (B) after media exchange.

potentiostat performance specifications.

When connected to a microbial electrochemical cell for a practical evaluation of an MESe application, the potentiostat operated as expected and produced accurate results that were comparable to literature values in terms of peak currents for the substrate. The microcontroller used in the design is programmable using C/C++ coding language, and thus allows flexibility to be customised for various applications.

Overall, it was concluded that the presented potentiostat design can be built and can provide accurate and precise measurements while being simple and affordable, as are especially important for prospective MESe applications. This would be important to improved response times for VFA measurements in AD. Future improvements of the design could attempt to increase current generation for measurement, as well as making the design robust for application during in field monitoring at large scale biogas facilities.

Credit authorship contribution statement

Andrew Hill; Conceptualization, Methodology, Visualisation, Data curation, Investigation, Writing – Original Draft, Presentation, Formal analysis, Writing – Review & Editing. **Stephan Tait;** Conceptualization, Writing – Review & Editing, Resources, Supervision. **Peter Harris;** Conceptualization, Writing – Review & Editing, Supervision. **Craig Ballie;** Conceptualization, Resources, Writing – Review & Editing, Supervision. **Bernardino Virdis;** Visualization, Writing – Review & Editing. **Bernadette McCabe;** Conceptualization, Writing – Review & Editing, Supervision.

Funding

This research did not receive any specific grant from funding agencies in the public, commercial, or not-for-profit sectors.

Declaration of Competing Interest

The authors declare that they have no known competing financial interests or personal relationships that could have appeared to influence the work reported in this paper.

Data availability

The authors are unable or have chosen not to specify which data has been used.

Acknowledgements

The financial support for Andrew Hill is received from the Queensland Government's Advance Queensland Research Fellows program. Bernardino Virdis acknowledges the support of the ARC through grants FL170100086 and LP200200136.

Supplementary materials

Supplementary material associated with this article can be found, in the online version, at doi:10.1016/j.electacta.2023.143201.

References

[1] B.E. Logan, K. Rabaey, Conversion of wastes into bioelectricity and chemicals by using microbial electrochemical technologies, Science 337 (2012) 686–690.
[2] M.D. Dryden, A.R. Wheeler, DStat: a versatile, open-source potentiostat for electroanalysis and integration, PLoS ONE 10 (2015), e0140349.
[3] E.S. Friedman, M.A. Rosenbaum, A.W. Lee, D.A. Lipson, B.R. Land, L.T. Angenent, A cost-effective and field-ready potentiostat that poises subsurface electrodes to monitor bacterial respiration, Biosens. Bioelectron. 32 (2012) 309–313.
[4] O.S. Hoilett, J.F. Walker, B.M. Balash, N.J. Jaras, S. Boppana, J.C. Linnes, KickStat: a coin-sized potentiostat for high-resolution electrochemical analysis, Sensors (Basel) (2020) 20.
[5] G.N. Meloni, Building a microcontroller based potentiostat: a inexpensive and versatile platform for teaching electrochemistry and instrumentation, J. Chem. Educ. 93 (2016) 1320–1322.
[6] A. Hill, S. Tait, C. Baillie, B. Virdis, B. McCabe, Microbial electrochemical sensors for volatile fatty acid measurement in high strength wastewaters: a review, Biosens. Bioelectron. 165 (2020), 112409.
[7] E. Atci, J.T. Babauta, S.T. Sultana, H. Beyenal, Microbiosensor for the detection of acetate in electrode-respiring biofilms, Biosens. Bioelectron. 81 (2016) 517–523.
[8] F. Scarabotti, L. Rago, K. Buhler, F. Harnisch, The electrode potential determines the yield coefficients of early-stage Geobacter sulfurreducens biofilm anodes, Bioelectrochemistry 140 (2021), 107752.
[9] G. Pasternak, J. Greenman, I. Ieropoulos, Dynamic evolution of anodic biofilm when maturing under different external resistive loads in microbial fuel cells. Electrochemical perspective, J. Power Sources 400 (2018) 392–401.
[10] A. Vilajeliu-Pons, L. Baneras, S. Puig, D. Molognoni, A. Vila-Rovira, E. Hernandez-Del Amo, M.D. Balaguer, J. Colprim, External resistances applied to MFC affect core microbiome and swine manure treatment efficiencies, PLoS ONE 11 (2016), e0164044.
[11] A. Schievano, A. Colombo, A. Cossettini, A. Goglio, V. D'Ardes, S. Trasatti, P. Cristiani, Single-chamber microbial fuel cells as on-line shock-sensors for volatile fatty acids in anaerobic digesters, Waste Manag. 71 (2018) 785–791.
[12] A. Hassanein, F. Witarsa, S. Lansing, L. Qiu, Y. Liang, Bio-electrochemical enhancement of hydrogen and methane production in a combined anaerobic digester (AD) and microbial electrolysis cell (MEC) from dairy manure, Sustainability 12 (2020).
[13] T. Tommasi, G.P. Salvador, M. Quaglio, New insights in microbial fuel cells: novel solid phase anolyte, Sci. Rep. 6 (2016) 29091.
[14] X. Zhang, X. Xia, I. Ivanov, X. Huang, B.E. Logan, Enhanced activated carbon cathode performance for microbial fuel cell by blending carbon black, Environ. Sci. Technol. 48 (2014) 2075–2081.
[15] B. Korth, F. Harnisch, Spotlight on the energy harvest of electroactive microorganisms: the impact of the applied anode potential, Front. Microbiol. 10 (2019) 1352.
[16] J. Kretzschmar, P. Böhme, J. Liebetrau, M. Mertig, F. Harnisch, Microbial electrochemical sensors for anaerobic digestion process control - Performance of electroactive biofilms under real conditions, Chem. Eng. Technol. 41 (2018) 687–695.
[17] X.G. Guo, J.B. Jia, H. Dong, Q.Y. Wang, T. Xu, B.Y. Fu, R. Ran, P. Liang, X. Huang, X.Y. Zhang, Hydrothermal synthesis of Fe-Mn bimetallic nanocatalysts as high-efficiency cathode catalysts for microbial fuel cells, J. Power Sources 414 (2019) 444–452.

[18] I. Anshori, G.F. Mufiddin, I.F. Ramadhan, E. Ariasena, S. Harimurti, H. Yunkins, C. Kurniawan, Design of smartphone-controlled low-cost potentiostat for cyclic voltammetry analysis based on ESP32 microcontroller, Sens. Biosens. Res. 36 (2022).
[19] A.V. Cordova-Huaman, V.R. Jauja-Ccana, A.La Rosa-Toro, Low-cost smartphone-controlled potentiostat based on Arduino for teaching electrochemistry fundamentals and applications, Heliyon 7 (2021) e06259.
[20] Y.C. Li, E.L. Melenbrink, G.J. Cordonier, C. Boggs, A. Khan, M.K. Isaac, L. K. Nkhonjera, D. Bahati, S.J. Billinge, S.M. Haile, R.A. Kreuter, R.M. Crable, T. E. Mallouk, An easily fabricated low-cost potentiostat coupled with user-friendly software for introducing students to electrochemical reactions and electroanalytical techniques, J. Chem. Educ. 95 (2018) 1658–1661.
[21] C. Kazadi Mbamba, X. Flores-Alsina, D. John Batstone, S. Tait, Validation of a plant-wide phosphorus modelling approach with minerals precipitation in a full-scale WWTP, Water Res. 100 (2016) 169–183.
[22] J.R. Kim, B. Min, B.E. Logan, Evaluation of procedures to acclimate a microbial fuel cell for electricity production, Appl. Microbiol. Biotechnol. 68 (2005) 23–30.
[23] D. Kashyap, P.K. Dwivedi, J.K. Pandey, Y.H. Kim, G.M. Kim, A. Sharma, S. Goel, Application of electrochemical impedance spectroscopy in bio-fuel cell characterization: a review, Int. J. Hydrogen Energ. 39 (2014) 20159–20170.
[24] R. Trouillon, D. O'Hare, Comparison of glassy carbon and boron doped diamond electrodes: resistance to biofouling, Electrochim. Acta 55 (2010) 6586–6595.
[25] C. Gimkiewicz, F. Harnisch, Waste water derived electroactive microbial biofilms: growth, maintenance, and basic characterization, J. Vis. Exp. (2013) 50800.
[26] A. Okamoto, K. Saito, K. Inoue, K.H. Nealson, K. Hashimoto, R. Nakamura, Uptake of self-secreted flavins as bound cofactors for extracellular electron transfer in Geobacter species, Energy Environ. Sci. 7 (2014) 1357–1361.
[27] A.J. Bard, L.R. Faulkner, Electrochemical Methods, Fundamentals and Applications, 2nd Edition ed., John Wiley & Sons2001.
[28] D.L. Langhus, Analytical Electrochemistry, 2nd Edition, 78, (Wang, Joseph), Journal of Chemical Education, 2001, p. 457.
[29] D. Harvey, Electrochemical Methods, Analytical Chemistry, Springer, Berlin/ Heidelberg, Germany, 2011, pp. 667–782.
[30] M.W. Glasscott, M.D. Verber, J.R. Hall, A.D. Pendergast, C.J. McKinney, J.E. Dick, SweepStat: a build-it-yourself, two-electrode potentiostat for macroelectrode and ultramicroelectrode studies, J. Chem. Educ. 97 (2019) 265–270.
[31] P. Irving, R. Cecil, M.Z. Yates, MYSTAT: a compact potentiostat/galvanostat for general electrochemistry measurements, Hardwarex 9 (2021).
[32] X. Jing, X. Liu, C. Deng, S. Chen, S. Zhou, Chemical signals stimulate Geobacter soli biofilm formation and electroactivity, Biosens. Bioelectron. 127 (2019) 1–9.
[33] T. Ueki, K.P. Nevin, T.L. Woodard, M.A. Aklujkar, D.E. Holmes, D.R. Lovley, Construction of a Geobacter strain with exceptional growth on cathodes, Front. Microbiol. 9 (2018) 1512.
[34] S. Yadav, S.A. Patil, Microbial electroactive biofilms dominated by Geoalkalibacter spp. from a highly saline-alkaline environment, npj Biofilms Microbiomes 6 (2020) 38.
[35] X. Jin, X. Li, N. Zhao, I. Angelidaki, Y. Zhang, Bio-electrolytic sensor for rapid monitoring of volatile fatty acids in anaerobic digestion process, Water Res. 111 (2017) 74–80.
[36] J. Kretzschmar, C. Koch, J. Liebetrau, M. Mertig, F. Harnisch, Electroactive biofilms as sensor for volatile fatty acids: cross sensitivity, response dynamics, latency and stability, Sensor. Actuat. B-Chem. 241 (2017) 466–472.
[37] A. Baudler, S. Riedl, U. Schroder, Long-term performance of primary and secondary electroactive biofilms using layered corrugated carbon electrodes, Front. Energy Res. 2 (2014).
[38] Y. Liu, F. Harnisch, K. Fricke, R. Sietmann, U. Schroder, Improvement of the anodic bioelectrocatalytic activity of mixed culture biofilms by a simple consecutive electrochemical selection procedure, Biosens. Bioelectron. 24 (2008) 1012–1017.
[39] Y. Jiang, N. Chu, R.J. Zeng, Submersible probe type microbial electrochemical sensor for volatile fatty acids monitoring in the anaerobic digestion process, J. Clean. Prod. 232 (2019) 1371–1378.
[40] G.Q. Zhang, Y.F. Zhou, F.L. Yang, Hydrogen production from microbial fuel cells-ammonia electrolysis cell coupled system fed with landfill leachate using Mo2C/N-doped graphene nanocomposite as HER catalyst, Electrochim. Acta 299 (2019) 672–681.
[41] H. Sun, Y. Zhang, S. Wu, R. Dong, I. Angelidaki, Innovative operation of microbial fuel cell-based biosensor for selective monitoring of acetate during anaerobic digestion, Sci. Total Environ. 655 (2019) 1439–1447.